

Effects of Multiphase Flow on Internal CO₂ Corrosion of Mild Steel Pipelines

S. Nestic*

Institute for Corrosion and Multiphase Technology, Ohio University, Athens, Ohio 45701, United States

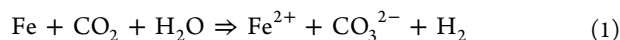
ABSTRACT: The focus in this paper is on the effects of multiphase flow on CO₂ corrosion of mild steel pipelines. The significance of mass transfer in turbulent flow is discussed first: (i) when an increased rate of mass transfer of corrosive species, such as H⁺ ions, to the steel surface leads to an acceleration of the cathodic reactions and a higher corrosion rate and (ii) when an increased mass-transfer rate of the corrosion product, ferrous ions (Fe²⁺), away from the steel surface makes it harder to form protective ferrous carbonate layers. The mechanical interaction of the flow with the pipe walls is discussed next, where the wall shear stress is often blamed for removal of protective surface layers, such as iron carbonate or inhibitor films. Using macroscopic as well as atomic scale measurements [atomic force microscopy (AFM)], it was found that it is very unlikely that truly protective surface layers can be removed by mechanical forces alone. The other multiphase flow effects on corrosion, such as the effect of condensation on the top of the line corrosion (TLC) in wet gas pipelines, the effect of water settling and wetting in oil-carrying lines, and the effects of sand on erosion–corrosion and underdeposit corrosion in production pipelines, are outlined at the end.

INTRODUCTION

Aqueous carbon dioxide (CO₂) corrosion is usually associated with oil and gas pipelines made from mild steel. It becomes a serious issue when, in oil and gas production and transportation, significant amounts of CO₂ and water are present. CO₂ is very soluble in water, where it forms carbonic acid (H₂CO₃), which attacks mild steel.¹ Despite thousands of papers published on CO₂ corrosion in the literature, one cannot easily piece together a picture of CO₂ corrosion, because much of the useful information is scattered. Recently, two papers were published in mainstream corrosion handbooks, which represent a compilation of the current understanding on this subject, covering the basic processes and mechanisms.^{2,3} In the present paper, the focus is on the effects of multiphase flow on CO₂ corrosion of mild steel pipelines.

FUNDAMENTALS OF UNIFORM CO₂ CORROSION OF MILD STEEL IN AQUEOUS SOLUTIONS

For the case of mild steel, one can write the overall CO₂ corrosion reaction as



As iron, Fe, from the steel is oxidized to ferrous ions, Fe²⁺, in the presence of CO₂ and water, H₂O, hydrogen gas, H₂, is evolved as a result of the reduction of hydrogen ions, H⁺.

The CO₂ gas is rather soluble in water. In terms of volumetric molar concentrations, almost as much CO₂ can be found in the aqueous phase as in the gas phase. Only a rather small fraction (approximately 0.2%) of the dissolved CO₂ molecules is hydrated to form a “weak” carbonic acid, H₂CO₃. This and other important homogeneous chemical reactions occurring in an aqueous CO₂ solution are listed in Table 1. The equilibrium “constants” for these reactions typically depend upon the temperature and, in some cases, pressure and ionic strength of the solution.⁴

Table 1. Key Chemical Reactions Occurring in an Aqueous CO₂-Saturated Solution

name	reaction
dissolution of carbon dioxide	$\text{CO}_{2(\text{g})} \xrightleftharpoons{K_{\text{sol}}} \text{CO}_2 \quad (2)$
carbon dioxide hydration	$\text{CO}_2 + \text{H}_2\text{O} \xrightleftharpoons{K_{\text{hy}}} \text{H}_2\text{CO}_3 \quad (3)$
carbonic acid dissociation	$\text{H}_2\text{CO}_3 \xrightleftharpoons{K_{\text{ca}}} \text{H}^+ + \text{HCO}_3^- \quad (4)$
bicarbonate anion dissociation	$\text{HCO}_3^- \xrightleftharpoons{K_{\text{bi}}} \text{H}^+ + \text{CO}_3^{2-} \quad (5)$
water dissociation	$\text{H}_2\text{O} \xrightleftharpoons{K_{\text{wa}}} \text{H}^+ + \text{OH}^- \quad (6)$

Some reactions listed in Table 1, such as, for example, the dissociation of carbonic acid, are very fast, while others, such as the CO₂ dissolution in water and the hydration of dissolved CO₂, are much slower and can become the rate-determining step, thereby limiting the magnitude of the corrosion rate.

The main heterogeneous reduction/oxidation reactions occurring at the steel surface (the electrochemical reactions), which are “behind” the CO₂ corrosion of mild steel, are listed in Table 2. The electrochemical dissolution of iron from the steel, reaction 7 in Table 2, is the main oxidation (anodic) reaction in aqueous CO₂ corrosion. The iron dissolution reaction is more complicated than it appears in Table 2. For example, the two electrons are not “released” in one step; rather a sequence of intermediate steps occurs, which all add up to the overall reaction. These and many other details on the mechanism of the iron dissolution reaction can be found in the literature.^{5–7} The rate of the active dissolution of iron, reaction 7 in Table 2,

Special Issue: Upstream Engineering and Flow Assurance (UEFA)

Received: February 15, 2012

Revised: June 11, 2012

Published: June 11, 2012

Table 2. Main Electrochemical Reactions Behind Mild Steel Corrosion in Aqueous CO₂ Solutions

name	reaction
anodic dissolution (oxidation) of iron	$\text{Fe} \rightarrow \text{Fe}^{2+} + 2\text{e}^-$ (7)
cathodic hydrogen evolution by reduction of dissociated (free) hydrogen ions	$2\text{H}^+ + 2\text{e}^- \rightarrow \text{H}_2$ (8)
cathodic hydrogen evolution by reduction of water	$2\text{H}_2\text{O} + 2\text{e}^- \rightarrow \text{H}_2 + 2\text{OH}^-$ (9)
cathodic hydrogen evolution by reduction of carbonic acid	$2\text{H}_2\text{CO}_3 + 2\text{e}^- \rightarrow \text{H}_2 + 2\text{HCO}_3^-$ (10)
cathodic hydrogen evolution by reduction of bicarbonate ion	$2\text{HCO}_3^- + 2\text{e}^- \rightarrow \text{H}_2 + 2\text{CO}_3^{2-}$ (11)

is independent from flow and mass transfer and is not a strong function of pH nor p_{CO_2} but does depend upon temperature.

The main cathodic reaction in acidic corrosion is the reduction of the dissociated (free) hydrogen ions, H^+ , according to the overall reaction 8, given in Table 2. The rate of hydrogen evolution, reaction 8, primarily depends upon pH; however, it is often limited by the rate at which H^+ ions can be transported from the bulk solution to the steel surface by mass transfer (often referred to as diffusion, hence the term diffusion limitation). This makes this reaction rate “flow sensitive”, which really refers to the fact that turbulent flow can increase the mass-transfer rate of H^+ ions and indirectly the rate of the hydrogen evolution reaction and ultimately corrosion.

For the pH range seen in typical CO₂ saturated aqueous solutions ($4 < \text{pH} < 6$), this limiting diffusion rate is rather small, because of a relatively low concentration of H^+ ions in the bulk. The presence of dissolved CO₂ in water increases the corrosion rate primarily by making it easier for hydrogen to evolve from water.

The so-called “direct reduction of water”, i.e., the reduction of H^+ ions from the water molecules adsorbed on the steel surface, reaction 9 in Table 2, is thermodynamically equivalent to the hydrogen evolution reaction 8. However, this pathway for hydrogen evolution is comparatively slow (kinetically hindered) and cannot be used to explain the high corrosion rates seen in CO₂ saturated aqueous solutions.⁸

When dissolved CO₂ is hydrated to form a weak H₂CO₃, this enables hydrogen evolution at a much higher rate than would be found in an aqueous solution of a strong acid, at the same pH. The homogeneous dissociation of H₂CO₃ (see Table 1) provides additional H^+ ions, which can readily be reduced at the steel surface according to reaction 8.¹ A different pathway is also possible, where the H^+ ions are “directly” reduced from the H₂CO₃ molecules adsorbed on the steel surface, much in the same way as happens for adsorbed water molecules (see reaction 10 in Table 2). This is often referred to as “direct reduction of H₂CO₃”.^{9–13} Clearly, this hydrogen evolution reaction also amounts to reduction of H^+ ions from the adsorbed H₂CO₃ molecules and is thermodynamically equivalent to the other two hydrogen evolution reactions 8 and 9. For the three cases, the distinction is only in the pathway and, consequently, in the kinetics.

The rate of hydrogen evolution from H₂CO₃, reaction 10, is much faster than that from water, reaction 9. Because of the abundance of water and dissolved CO₂, there is a sufficiently large “reservoir” of H₂CO₃ and ultimately H^+ ions in a CO₂

saturated aqueous solution. This would lead to some very high corrosion rates were it not for the slow CO₂ hydration step (see reaction 3 in Table 1), which gives rise to chemical reaction-limiting rates for this cathodic reaction.^{10–15}

Because HCO₃[−] is another weak acid (it only partially dissociates to give CO₃^{2−}; see Table 1), then by analogy, one can assume that reduction of H^+ ions from HCO₃[−] is yet another pathway for hydrogen evolution,¹³ according to reaction 11 in Table 2. Again, this reaction is thermodynamically equivalent to the previous three pathways for hydrogen evolution, and the distinction is in the kinetics. Experimental evidence suggests that this pathway for hydrogen evolution is slower than direct reduction of H₂CO₃. However, in neutral and alkaline conditions, the concentration of HCO₃[−] can be much higher than that of H₂CO₃, and it is likely that an accelerated rate of reaction 11 can make it the dominant cathodic reaction in CO₂ saturated aqueous solutions at high pH. However, in the practical range of interest considered here ($4 < \text{pH} < 6$), the two concentrations are in the same range, and because of kinetic hindrance, the direct reduction of HCO₃[−] can be ignored.

This leaves only two significant possibilities for hydrogen evolution in CO₂ saturated aqueous solutions: reduction of the dissociated (free) H^+ ions, reaction 8, and reduction of H^+ ions from H₂CO₃, reaction 10. The former is a strong function of pH and flow, while the latter is a function of CO₂ partial pressure. Both are kinetically limited, reaction 8 by diffusion and reaction 10 by the slow CO₂ hydration step.

Under certain conditions, a ferrous carbonate, FeCO₃, layer can form in CO₂ corrosion of mild steel by precipitation and can reduce the corrosion rate.¹⁶ The cause for the precipitation of FeCO₃ is the high local concentrations of Fe²⁺ and CO₃^{2−} species in the aqueous solution. Most of the Fe²⁺ ions are provided by corrosion of mild steel (see reaction 7 in Table 2), while the CO₃^{2−} ions come from dissolved CO₂ (see reaction 5 in Table 1). When the product of Fe²⁺ and CO₃^{2−} species concentrations exceeds the so-called solubility limit, they form solid ferrous carbonate according to



where the solubility product constant, $K_{\text{sp}}(\text{FeCO}_3)$, is a function of the temperature and ionic strength.¹⁷

Because of corrosion, which releases ferrous ions, Fe²⁺, into the solution, the product of concentrations of Fe²⁺ and CO₃^{2−} ions in the aqueous solution is frequently much higher than the solubility limit. This is the case particularly at the steel surface, where the Fe²⁺ ions are generated and their concentration can be very high. The solubility limit is readily exceeded at low temperatures when the kinetics of reaction 12 is slow, leading to a departure from equilibrium termed supersaturation, defined as

$$\text{SS}_{(\text{FeCO}_3)} = \frac{(c_{\text{Fe}^{2+}})(c_{\text{CO}_3^{2-}})}{K_{\text{sp}}(\text{FeCO}_3)} \quad (13)$$

The FeCO₃ precipitation starts by heterogeneous nucleation, a process that happens relatively fast because of the many imperfections on the surface of the steel, which serve as good nucleation sites. Nucleation is followed by crystalline FeCO₃ layer growth. The rate of precipitation on the steel surface is therefore limited by the rate of crystal growth, which can be

expressed as a function of supersaturation, surface area, and temperature.¹⁶

Scanning electron microscopy (SEM) images of a crystalline ferrous carbonate layer formed on a mild steel substrate are shown in Figure 1. When the FeCO_3 layer is dense, it can slow

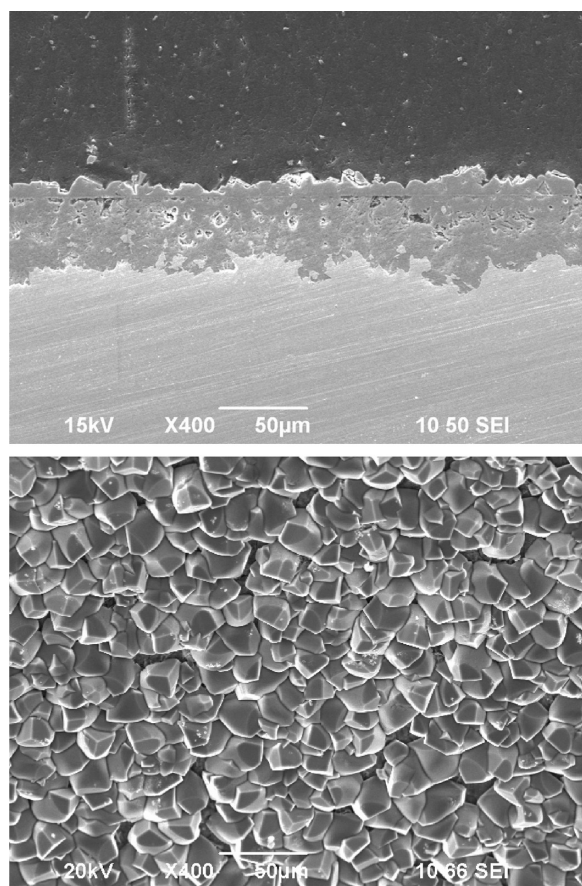


Figure 1. Cross-sectional and top-view SEM images of a ferrous carbonate layer formed on mild steel, at 80 °C, pH 6.6, $p_{\text{CO}_2} = 0.5$ bar, and stagnant conditions.

the corrosion process by presenting a transport barrier for the corrosive species. Protection from corrosion is also achieved by the so-called “coverage” of the surface; i.e., in places where the FeCO_3 crystals adhere to the steel surface, there is little or no corrosion. This is clearly shown in the higher magnification transmission electron microscopy (TEM) image of a cross-section produced using the focused ion beam (FIB) technique (see Figure 2a), where the attack on the steel seems to proceed only in “between” the FeCO_3 crystals (area B in Figure 2a, magnified in panels b and c of Figure 2). In the presence of dense FeCO_3 layers, the conditions at the steel surface are different compared to those in the bulk. The pH is much higher, which may lead to the formation of other solids, such as oxides and hydroxides. Small amounts of magnetite, Fe_3O_4 , are sometimes detected particularly at high pH and temperature, as shown in panels b and c of Figure 2, which leads to an even better protection from corrosion.

Having defined above the main chemical processes underlying CO_2 corrosion of mild steel in aqueous solutions, we can now consider the effects of turbulent flow and, in particular, multiphase flow, frequently present in oil and gas pipelines. Some of the main ways in which flow affects the aqueous CO_2

corrosion of mild steel pipelines are discussed in the following section. In many instances, it is impossible to fully separate one effect from the other, and there is no ideal way of presenting the overall situation. The main flow effects covered below are discussed in the context of the theory described above.

The direct effect of mass transfer in turbulent flow is described first, followed by the discussion of wall shear stress and the mechanical effects on protective surface layers. The other multiphase flow effects, such as the effect of condensation on the so-called top of the line corrosion (TLC) in wet gas pipelines, the effect of water wetting in oil carrying lines, and the effects of sand on erosion–corrosion and underdeposit corrosion in production pipelines, are outlined at the end; however, their detailed description exceeds the scope of this paper.

■ EFFECT OF MULTIPHASE FLOW ON AQUEOUS CO_2 CORROSION OF MILD STEEL

Mass-Transfer Effect. Turbulent flow enhances mass transport of species to and away from the mild steel internal pipe surface by affecting transport through the boundary layer.¹⁸ This general statement is true for single-phase water flow as well as multiphase flow. One can imagine two main scenarios where enhanced mass transfer affects the corrosion rate:

(1) An increased rate of transport of corrosive species, such as H^+ ions to the surface, leads to a lower surface pH and an acceleration of the cathodic reactions and a higher rate of corrosion (see reaction 8 in Table 2). This is particularly pronounced at lower bulk pH ($3 < \text{pH} < 5$) and/or at lower partial pressures of CO_2 ($p_{\text{CO}_2} \leq 1$ bar), when the concentration of H^+ ions is relatively high and controls the overall corrosion process (see Figure 3). It is worth repeating that the reduction of the other major cathodic species, H_2CO_3 , via reaction 10 in Table 2, is not very sensitive to changes in flow and mass transfer, because the surface concentration of H_2CO_3 is primarily affected by the slow hydration process, reaction 3 in Table 1. Therefore, very little sensitivity of the corrosion rate with respect to mass transfer is seen at $p_{\text{CO}_2} > 5$ bar (see Figure 4).

(2) An increased rate of mass transfer of the corrosion product, ferrous ions (Fe^{2+}), away from the steel surface makes it harder to form protective ferrous carbonate layers, according to reaction 12 as the surface concentration of Fe^{2+} ions decreases and approaches that of the bulk fluid. This effect can be compounded by the simultaneous decrease in the surface pH, as explained in the point above. Another associated effect is related to the removal of already formed protective ferrous carbonate layers by dissolution in an acidic solution; this process may be enhanced by flow and mass transfer, which sweeps the products of dissolution away from the surface.

There seems to be at least one other, more controversial, effect of flow and mass transfer on corrosion. Experimental evidence from laboratory studies suggests that turbulent flow may enhance the workings of corrosion inhibitors by making it easier for them to reach the steel surface. This effect may appear counterintuitive, because intense flow is most often perceived as adverse to corrosion inhibition, when it is suspected that the integrity of the very thin inhibitor layer at the steel surface may be compromised by the mechanical effects exerted by turbulent flow. This effect is discussed below.

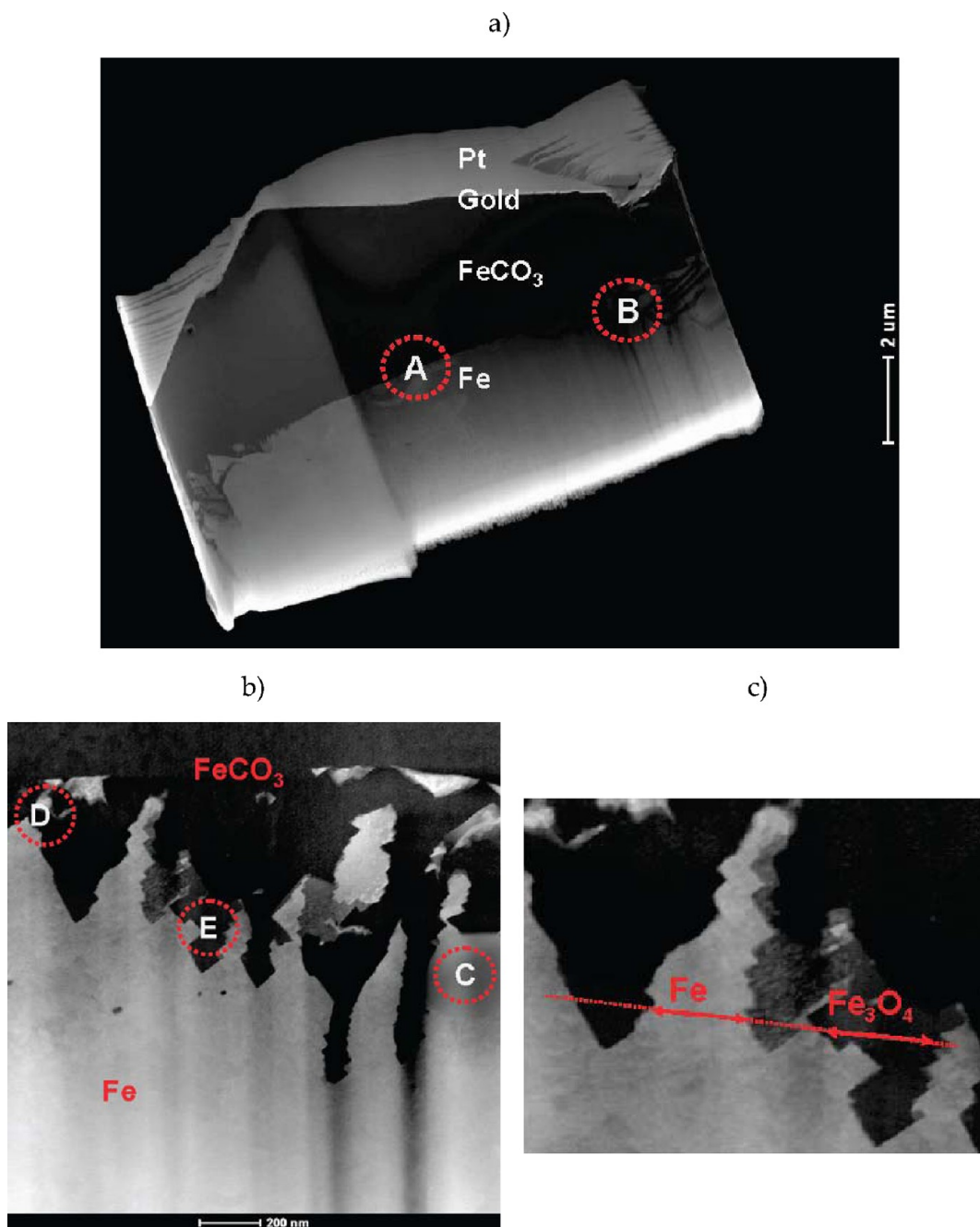


Figure 2. TEM of a ferrous carbonate crystal formed on mild steel, at 80 °C, pH 6.6, $p_{\text{CO}_2} = 0.5$ bar, and stagnant conditions: (a) cross-section “cutout” obtained using FIB, (b) enlarged location B, and (c) enlarged location E.

Effect of Mechanical Forces. The flow interaction with the internal pipe walls (where corrosion happens) can be described in terms of mechanical forces (stresses). Here, one can distinguish the normal stresses (pressure) and the shear stresses; then within each category, one may further consider the time-averaged (mean) value and the fluctuations. In turbulent flow and, particularly, in intermittent multiphase flow regimes (such as slug flow), the fluctuating component of the wall stress can be significant.

Wall Shear Stress. One can imagine a situation where the magnitude of the surface forces, which the fluid exerts on the internal pipe wall, exceeds the adhesive strength of the protective surface layers and leads to their failure and accelerated corrosion. In this scenario, it is usually the extreme

values of the shear stress that are deemed “responsible” for removal of protective surface layers, such as FeCO_3 or inhibitor films. While this is clearly a possibility, the question is how realistic is this scenario under the typical flow conditions encountered in oil and gas pipelines? As it turns out, there is only anecdotal field evidence about the effects of high shear stresses in CO_2 corrosion, which is usually complicated by many other contributing factors; therefore, one cannot formulate the answer with certainty. To establish whether wall shear forces can truly lead to failure of protective surface layers, one needs to compare the actual magnitude of the wall shear stress in multiphase flow to the adhesive strength of the protective layers. Neither is normally known, and only some recent laboratory studies shed light onto this subject matter.

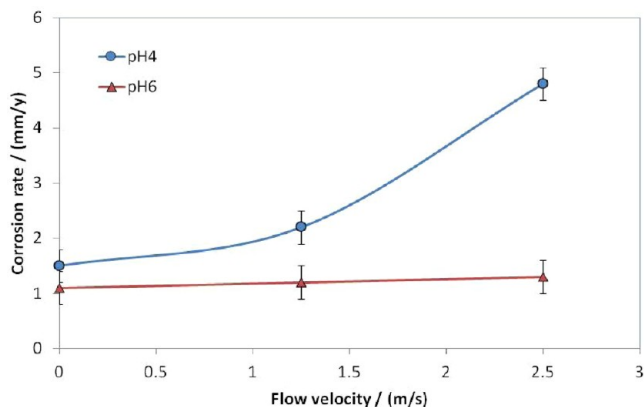


Figure 3. Effect of flow velocity and pH on CO_2 corrosion at $T = 80$ °C and $p_{\text{CO}_2} = 0.5$ bar.

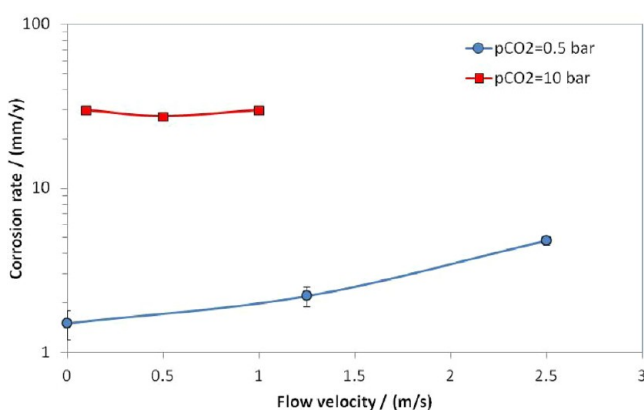


Figure 4. Effect of flow velocity and p_{CO_2} on CO_2 corrosion at $T = 50$ °C and pH 4.

Determining the wall shear stress in multiphase flow is no easy task. Credible models that exist for the various flow regimes are few and far apart. This is even more true for the slug flow regime, which is considered to be the most “violent”, with extreme fluctuations in the wall shear stress. Experimental results are also scarce, because creating a representative flow regime in a lab setting is challenging as one needs large-scale flow loops and multiphase flow capability. In such systems, the measurement of the wall shear stress can be performed using optical techniques, indirect techniques (such as flush-mounted hot-film or electrochemical mass-transfer probes), or direct floating-element-type devices. All of the techniques have their inherent strengths and weaknesses. Optical techniques, such as the particle image velocimetry (PIV), are very powerful; however, they are not easily adaptable to near wall measurements in multiphase flow and even less so for application near curved surfaces seen in pipes. Therefore, they will not be discussed here.

The indirect measurements using hot-film and electrochemical mass-transfer probes are comparatively simple to make and deploy. They are based on the Reynolds analogy of momentum and heat/mass transfer and therefore “suffer” from limitations associated with the theory behind it and are strictly valid only in fully developed turbulent flow. For practical reasons, heat-/mass-transfer elements used in these probes are relatively short, and it is not always possible to effectively eliminate the developing boundary layer effects. In intermittent multiphase flow, one cannot assume that there ever exists a fully

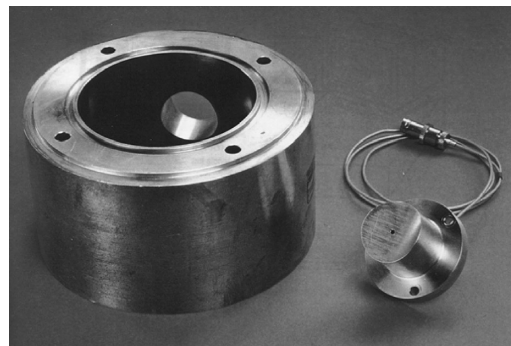


Figure 5. Pipe spool and the hot-film probe plug assembly.

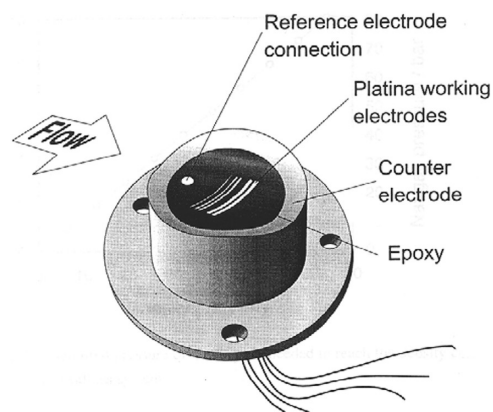


Figure 6. Sketch of the mass-transfer probe plug with multiple elements.

developed boundary layer. Therefore, in multiphase flow regimes and, in particular, in the slug flow regime, the application of heat-/mass-transfer techniques to measure wall shear stress produces results that have a significant degree of uncertainty. An example of these kinds of measurements is given in Figures 5–8. These experiments were performed in a gas-water flow in an inclinable 4 in. inner diameter multiphase flow loop equipped with a hot film (Figure 5), an electrochemical mass-transfer probe (Figure 6), and a transparent test section (Figure 7).

A composite image of a typical slug created in the slightly inclined uphill flow is shown in Figure 7. The same slug is presented in Figure 8a as a series of time lapse images recorded at a particular location in the test section. As the corresponding sample of the heat-/mass-transfer results presented in panels b and c of Figure 8 show, in slug flow, the time-averaged value of the wall shear stress is rather low (well below 100 Pa), with fluctuations associated with the passage of the slug front leading to short-lived peaks, which are 2–10 times higher in magnitude. It is possible that these extremes are even higher but cannot be detected because of their short duration with respect to the time constants associated with the heat-/mass-transfer measurements.

Alternative, direct measurements of wall shear stress in slug flow were made using a floating element sensor mounted on a mechanical cantilever with a micro-optical fiber Bragg grating (FBG) strain gage. While this technique has been “around” for many years, it is only recently that robust devices, such as the one shown in Figure 9, were developed that can be deployed in multiphase pipe flow. Initial measurements using this technique have shown even lesser variations of the wall shear stress with

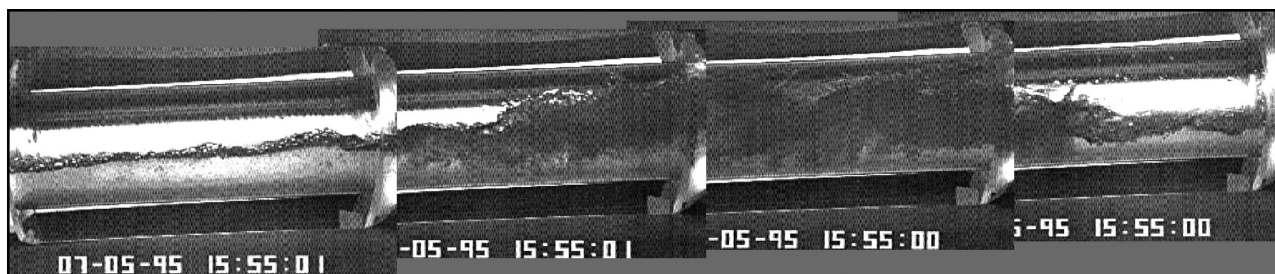


Figure 7. Composite image of a short liquid slug, where superficial velocity for water was $U_{sw} = 0.09$ m/s and for gas (air) was $U_{sg} = 2$ m/s, in 2° uphill flow in a 4 in. inner diameter line.

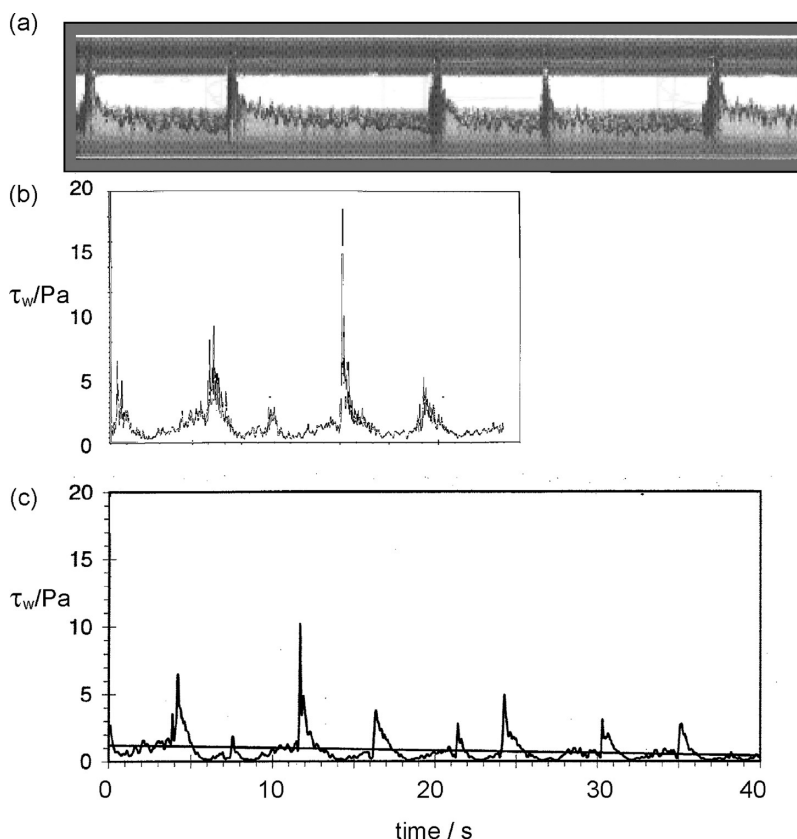


Figure 8. Slug flow: time series of the (a) video image, (b) wall shear stress measured with the hot-film probe, and (c) wall shear stress measured with the mass-transfer probe.

the passage of slugs, when compared to the indirect heat-/mass-transfer techniques presented above.

Given the uncertainties in measuring wall shear stress in multiphase flow, one must resign to an order-of-magnitude analysis and still try to answer the fundamental question: whether the extreme values in the wall shear stress could lead to mechanical damage of protective FeCO_3 layers or inhibitor films. To achieve that, measurements of adhesion strength of surface FeCO_3 layers and inhibitor films are required.

Adhesion Strength of Protective FeCO_3 Surface Layers. A long-term study that focused on removal of FeCO_3 layers identified two suitable techniques for the determination of the adhesion strength: one macroscopic technique and another atomic-scale technique. Macroscopic measurements were conducted by doing a typical tensile strength test, where a protective FeCO_3 layer developed on a mild steel surface was attached to an external steel stud using a strong adhesive and then pulled apart, while the force and deformation were

measured (see Figure 10). The atomic-scale measurements were conducted using atomic force microscopy (AFM), shown in Figure 11. The AFM cantilever was swept across the steel surface, and a single FeCO_3 crystal was imaged and then removed, while the magnitude of the shear force was recorded (see Figure 12).

The approximate value of the critical stress was calculated in both cases (from the tensile test and using AFM), and a remarkable agreement was achieved using these two vastly different techniques: the adhesion strength of the FeCO_3 layer was of the order of 10^7 Pa. Schmitt et al. have previously reported a similarly high strength of iron carbonate scale.¹⁹ This range of values when compared to the range of maximum wall shear stresses estimated for multiphase flow, which were of the order of 10^3 Pa, indicates a large “gap” of at least 4 orders of magnitudes, as shown in Figure 13. Clearly, it appears impossible that a wall shear stress seen in a realistic multiphase

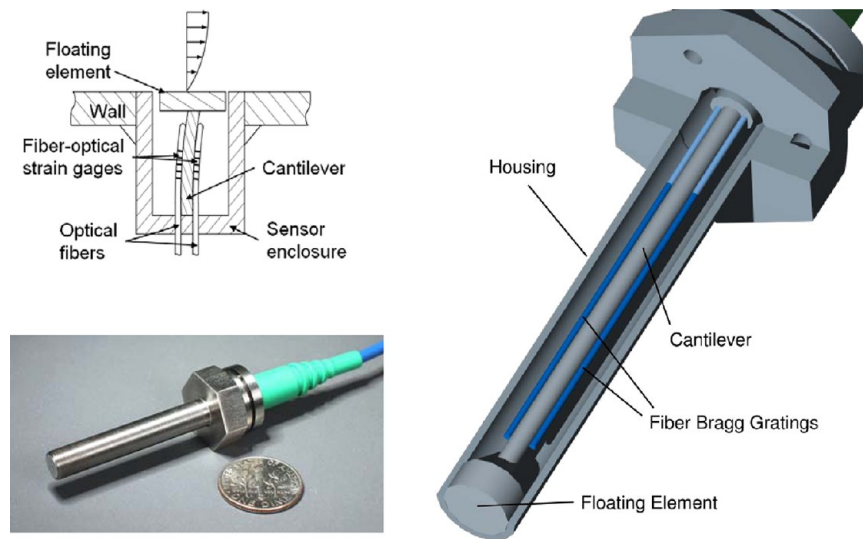


Figure 9. Floating element sensor mounted on a mechanical cantilever with a micro-optical FBG strain gage (by Lenterra with permission).

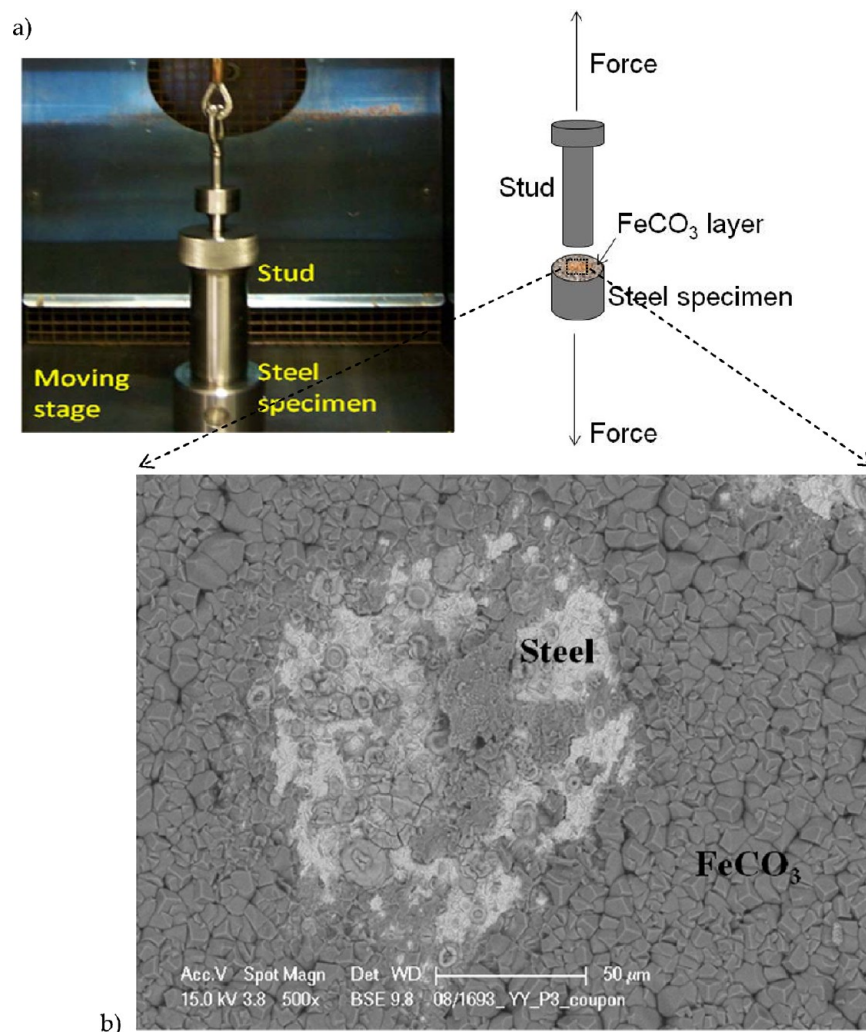


Figure 10. Mechanical strength test of a protective FeCO_3 layer developed on a mild steel specimen and attached to a steel stud using an adhesive: (a) experimental setup and (b) SEM of a steel surface after the test.

pipe flow can lead to pure mechanical removal of protective FeCO_3 layers.

On the other hand, field experience suggests that removal of protective FeCO_3 layers is generally possible, and this has been confirmed by selected laboratory experiments. We now know

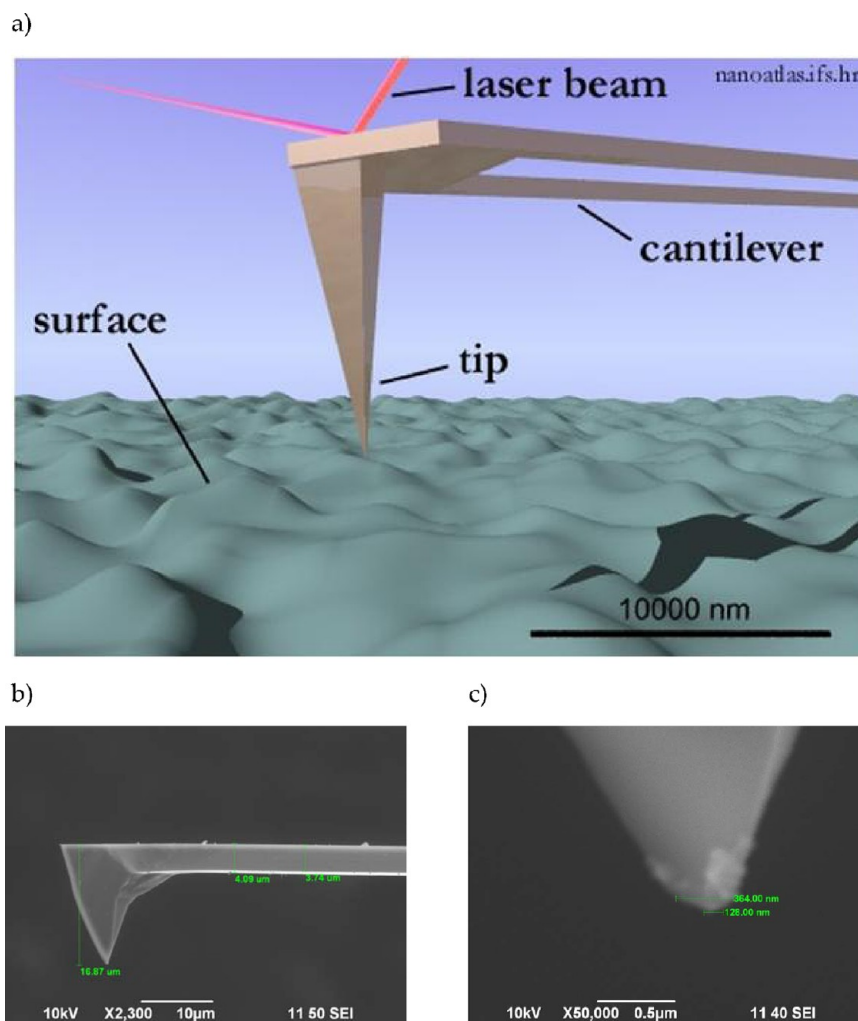


Figure 11. AFM: (a) schematic showing the basic working principle, (b) SEM of the cantilever and tip, and (c) enlarged view of the end of the tip.

that factors other than mechanical forces exerted by the flow must be involved for this to happen. It appears that the water chemistry plays a crucial role in removal of FeCO_3 layers. When conditions fall below the solubility limit for FeCO_3 , partial dissolution of FeCO_3 layers is seen, often leading to localized corrosion attack of the underlying mild steel. This can happen at lower pH ($\text{pH} < 6$), in the presence of organic acids (acetic, formic, propionic, etc.), with significant amount of NaCl ($\gg 1$ wt %), or because of dissolved oxygen ($\gg 1$ ppm). An example of a locally damaged FeCO_3 layer is given in Figure 14. It should be noted that the effect of chemical dissolution can be aggravated by flow, where the mechanical forces as well as enhanced mass transfer lead to an accelerated rate of protective FeCO_3 layer failure. In some instances, moderately protective FeCO_3 layers, which were poorly attached to the steel surface, could be removed by mechanical forces of the flow; however, this scenario has little practical relevance.

Adhesion Strength of Protective Corrosion Inhibitor Films.

A similar line of arguments, as presented above for the case of protective FeCO_3 layers, was considered for the case of corrosion inhibitor films. The addition of organic corrosion inhibitors is the most common way to combat internal corrosion of oil and gas pipelines made from mild steel. These long molecular chain surface-active chemicals form a very thin film at the steel surface and dramatically reduce the

corrosion rate (efficiency of 90% or more being quite common). Therefore, one of the main concerns is whether, in turbulent multiphase flow, these inhibitor films might be compromised or even fully removed by the mechanical stresses present at the pipe wall.

As was the case with protective FeCO_3 layers, the field experience does indicate some cases where inhibition failed to protect the internal pipe wall, and the blame was placed on “violent” flow conditions. Even if most of the anecdotes coming from the field suffer from so many complicating factors that it is hard to find a single convincing explanation for any given failure, the perception that high wall shear stresses present in multiphase flow can damage inhibitor films is widespread. This is so much so that laboratory testing procedures for inhibitor performance routinely include testing under very violent flow conditions. Examples are impinging jet and rotating cage experimental flow systems. In the former, a very high velocity stream of water is directed at an inhibited mild steel target, while in the latter, a cylindrical “cage”, made up of a series of steel specimen, is spun at a very high velocity in a vessel containing inhibited water. In both cases, inhibition failure can be achieved but usually only at extreme conditions, when the achieved wall shear stresses exceed those that can be found in realistic multiphase pipe flow, by many orders of magnitude.

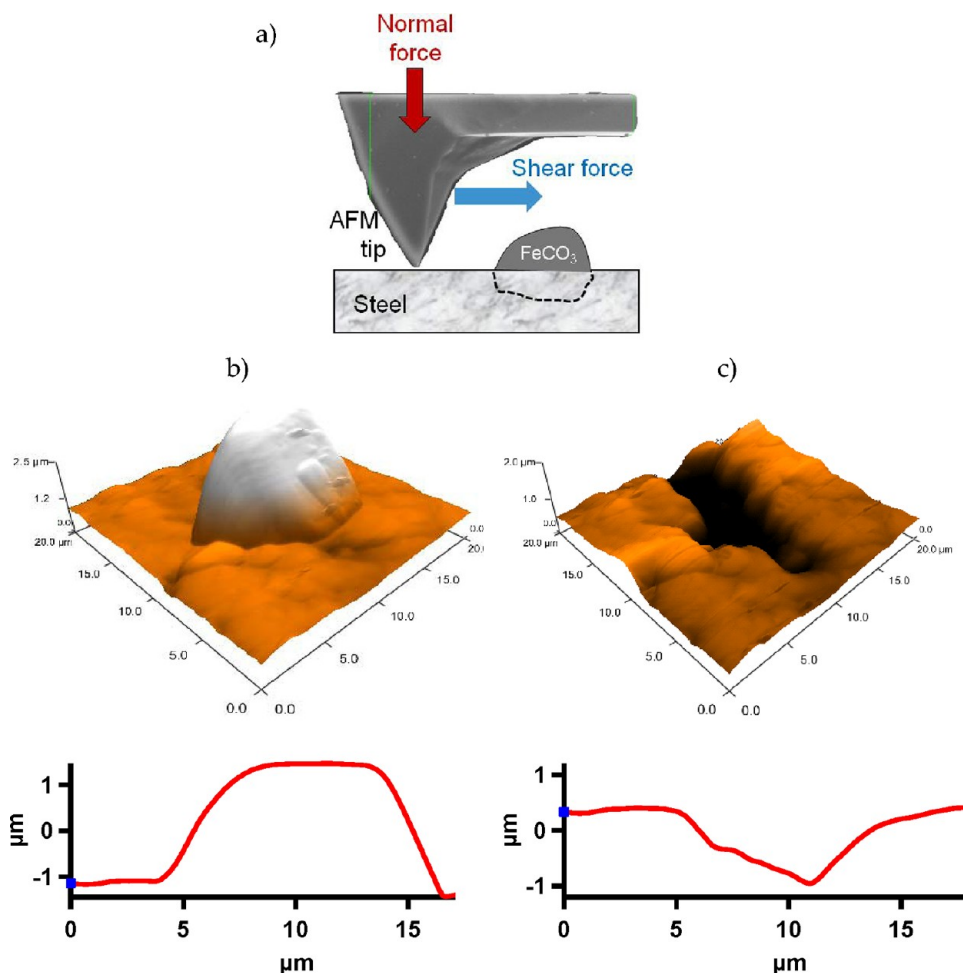


Figure 12. Removal of a single FeCO₃ crystal from a mild steel surface using a shear force applied by an AFM cantilever: (a) sketch of the experimental setup and AFM images and linear profile of the surface (b) before removal and (c) after removal.

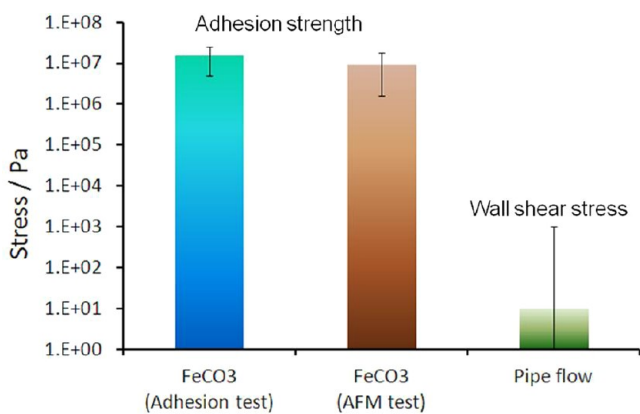


Figure 13. Comparison between the measured adhesion strength of a protective FeCO₃ layer and typical wall shear stress seen in multiphase pipe flow.

This makes conclusions from such experimentation dubious, yet the practice is prevalent in the industry.

Therefore, the question to be asked is whether the maximum realistic wall shear stresses estimated for multiphase pipe flow, which are on the order of 10³ Pa, can lead to mechanical failure of the very thin corrosion inhibitor films. This was investigated in a laboratory setting using AFM. A mild steel sample was exposed to inhibited water. The layer of inhibitor molecules

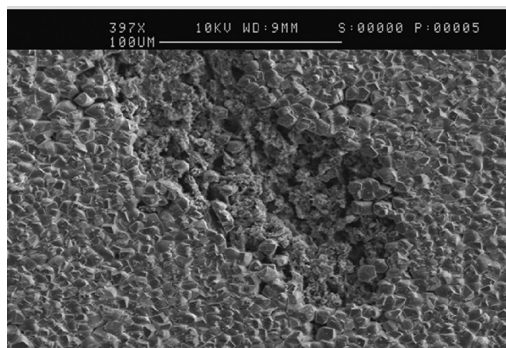


Figure 14. SEM image showing an example of localized damage to a protective FeCO₃ layer because of partial chemical dissolution, leading to localized attack of the underlying mild steel.

was first imaged, then mechanically removed using the AFM cantilever and tip, and then imaged again.

This procedure was developed and perfected initially using mica as a substrate, because the mica surface is atomically flat and enables better imaging of the very thin inhibitor film, which adsorbs on the surface. The results obtained using an imidazoline-based generic inhibitor formulation are shown in Figure 15. One can clearly see the patch of the surface where the inhibitor layer was “scratched off” by lateral movements of the AFM tip (Figure 15b). Profiling the surface after the scratch

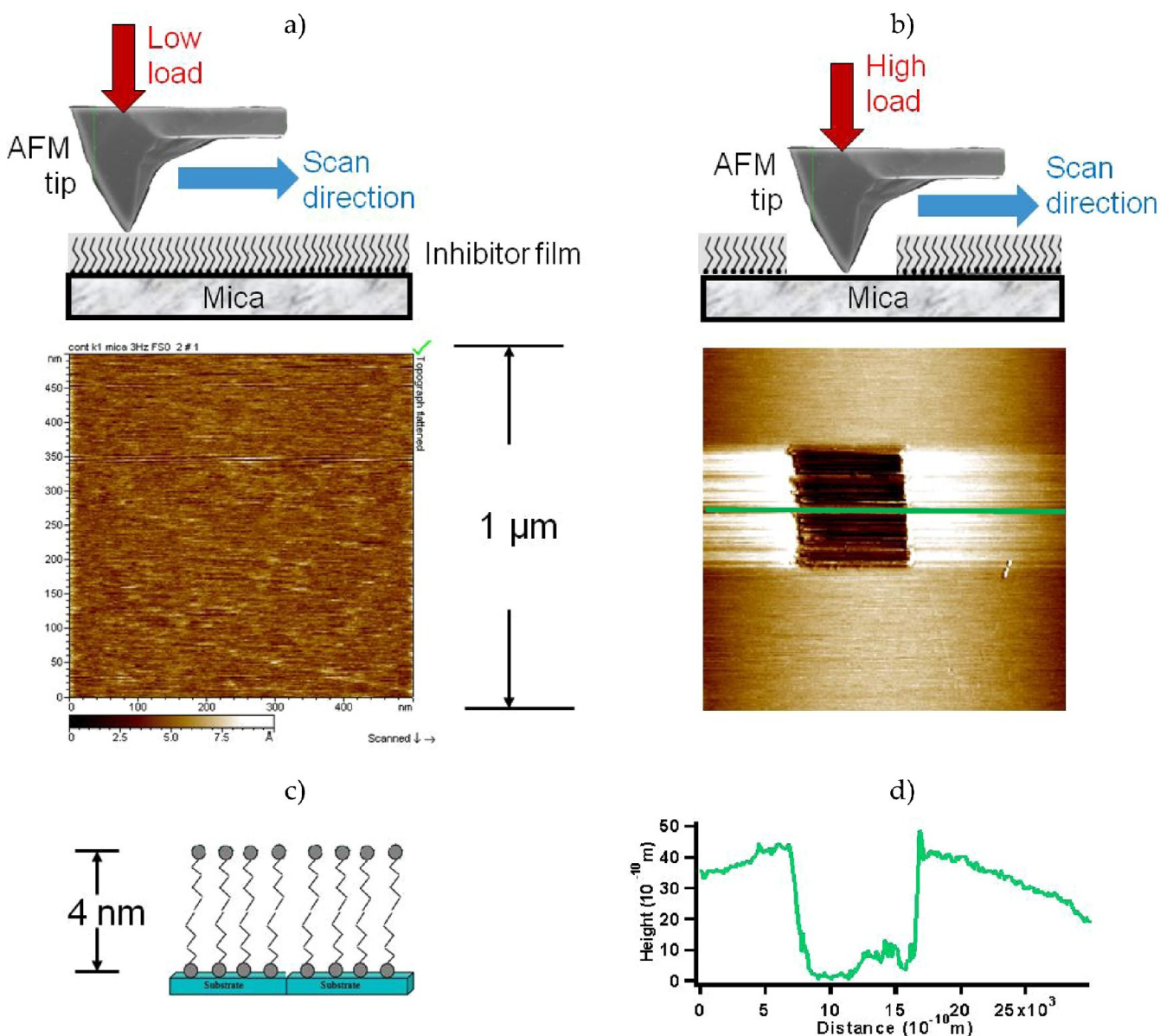


Figure 15. AFM analysis of a mica surface covered by an imidazoline-based inhibitor film: (a) topographic image of an “intact” surface, (b) topographic image of the “scratched” surface, (c) sketch of the double-layer inhibitor film structure, and (d) profile of the “scratched” surface.

enabled us to identify that the inhibitor film was about 4 nm thick (Figure 15d). Given that the length of the imidazoline inhibitor molecule used is about 2 nm, it was concluded that a bilayer of inhibitor formed on the mica surface (see sketch in Figure 15c). Similar experiments were then conducted on a mild steel surface, and the results are shown in Figure 16. Very tedious polishing was required to obtain the steel surface smooth enough so that AFM measurements could be performed at all, yet the surface is still much rougher than that of mica, as shown in Figure 16. Therefore, it is harder to clearly image the adsorbed inhibitor film on steel and identify the effects of “scratching”. However, from Figure 16, one can still estimate that the thickness of the imidazoline film on mild steel is still about 4 nm, suggesting again an adsorbed bilayer. What is more important is that the forces were measured as the inhibitor film was penetrated with the AFM tip and then again when the inhibitor film was “scratched off” by lateral movements of the tip. When recalculated, it was found that the normal stress required to penetrate the inhibitor film on

mild steel was on the order of 10^6 Pa (similar values were obtained for mica as a substrate). More importantly, the shear stress needed to scratch off the inhibitor layer from mild steel was estimated to be in the range of 5×10^7 Pa (while on mica, it was about half that value). Either way, it can be said that the adhesion strength of the inhibitor layer was on the order of 10^6 – 10^7 Pa, which is many orders of magnitude higher than the maximum wall shear stress seen in “violent” multiphase flow, which is estimated to be on the order of 10^3 Pa. Even if one factors in a significant safety margin, by assuming that both types of measurements have a significant error margin (e.g., an order of magnitude), one still cannot imagine that multiphase flow could lead to pure mechanical failure of protective inhibitor layers.

When a failure of an inhibitor to protect in multiphase flow is recorded in a laboratory investigation or is indicated from a field case study, it is advisable to look beyond the wall shear stress for a culprit. Many effects associated with multiphase flow could be at play, such as failure of the inhibitor to partition

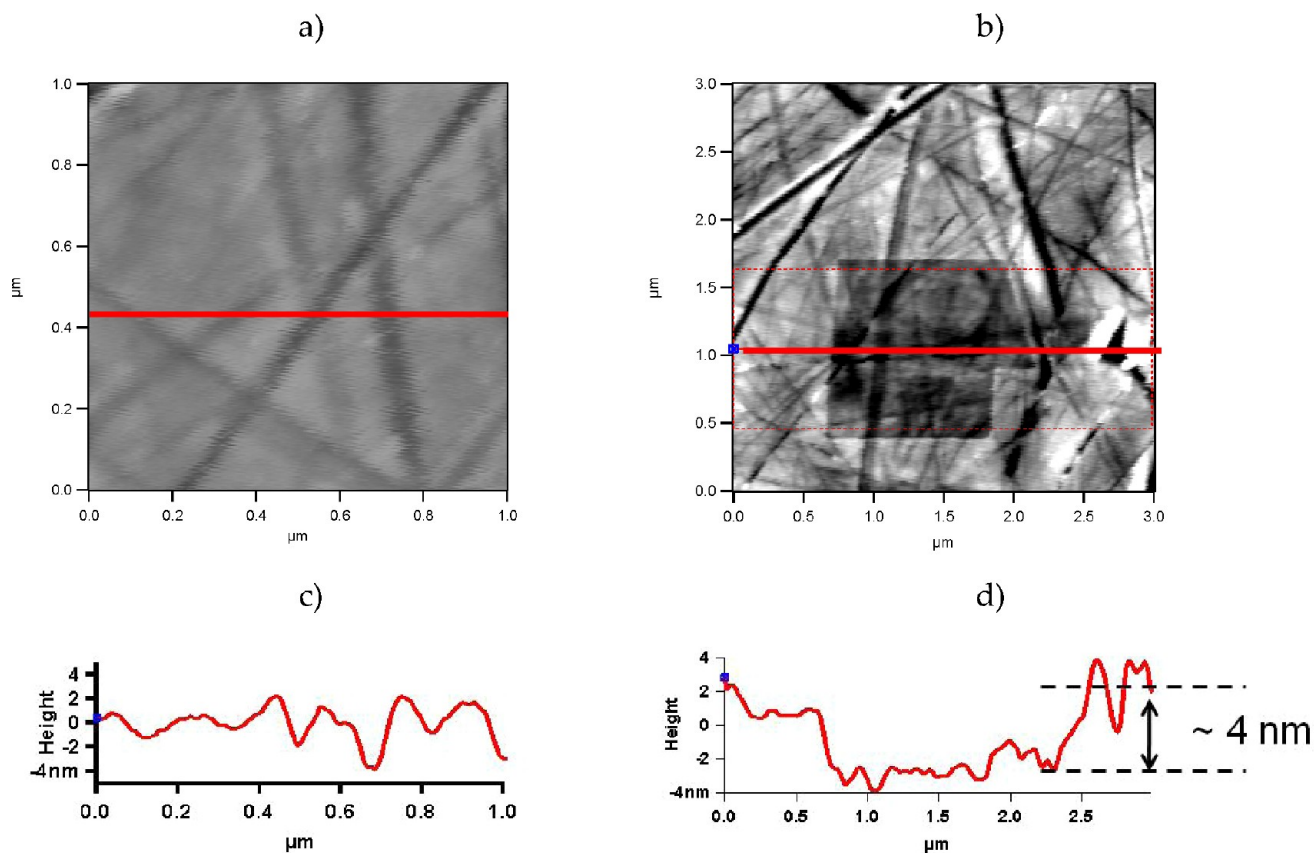


Figure 16. AFM analysis of a highly polished mild steel surface covered by an imidazoline-based inhibitor film: (a) topographic image of an “intact” surface, (b) topographic image of the “scratched” surface, (c) profile of the “intact” surface, and (d) profile of the “scratched” surface.

correctly into the water phase, accumulation of the inhibitor at the fluid/fluid or fluid/gas interface, making it unavailable to adsorb and protect the steel surface, preferential adsorption of the inhibitor on solids present in the multiphase stream, etc.

In a related laboratory study, an attempt was made to directly challenge this conclusion. A number of different flow systems was set up, using small-scale (2 L glass cells) and large-scale (2000 L multiphase flow loops, 4 in. inner diameter) equipment. An attempt was made, in carefully controlled experiments, to compromise the performance of the inhibitor film by relying solely on the mechanical wall forces created by the flow. Different flow patterns were investigated: (1) single-phase rotating cylinder flow in water, (2) jet impingement using water flow, (3) jet impingement using water–gas two-phase flow (see Figure 17a), (4) jet impingement using cavitating water–vapor two-phase flow (see Figure 17b), (5) single-phase pipe flow, (6) multiphase pipe flow or gas–water stratified flow (see Figure 17c), (7) multiphase pipe flow or slug flow (see Figure 17d), and (8) erosive water–sand slurry flow.

In situ measurements were made using electrochemical corrosion monitoring techniques as well as quartz crystal microbalance-based techniques, which can directly detect adsorption and removal of an inhibitor film. The results from many different experiments all led to the same conclusion: protective inhibitor films could not be removed by mechanical forces found in realistic multiphase pipe flow.

An example of the results is shown in Figure 18, where the flow in a 4 in. inner diameter acrylic pipe was changed from single-phase pipe flow to the so-called “standing-slug” or “hydraulic jump” flow (see Figure 17d), where the flow of gas

and water is manipulated to create a churning body of water, which visually resembles a true moving slug and yet “stands in place”. In the present case, the standing slug was positioned directly above an electrochemical quartz microbalance sensor, which can measure the corrosion rate and amount of adsorbed inhibitor *in situ*. The expectation was that the standing slug will create a continuously aggravated condition for inhibitor performance. One can see in Figure 18 that the introduction of the standing slug did lead to a short-lived decrease in the adsorbed inhibitor amount on the corroding iron surface. This resulted in a temporary loss of corrosion protection; however, within a few hours, the situation was restored to “normal” even if the standing slug remained in place. On the basis of other related experiments, it is believed that this brief loss of inhibition was due to the introduction of a large number of gas bubbles to the immediate vicinity of the corroding surface, which led to a temporary migration of the inhibitor from the steel–water interface to the gas–water interface. Similar results, where the flow was unable to mechanically remove the inhibitor, were obtained in many repeated experiments and in many different experimental setups. Such “unexpected” results were first indicated in a previous study by Gulbrandsen et al.²⁰

It should be noted that, in some instances, the findings were truly unexpected. For example, it was found that highly turbulent flow multiphase conditions led to better performance of corrosion inhibitors, probably because of intense mass transfer helping the inhibitor reach the pipe wall. Another example is the case of dilute sand slurry erosion, where the performance of the corrosion inhibitor was not impaired by impinging sand particles in the range of flow velocities of 1–4

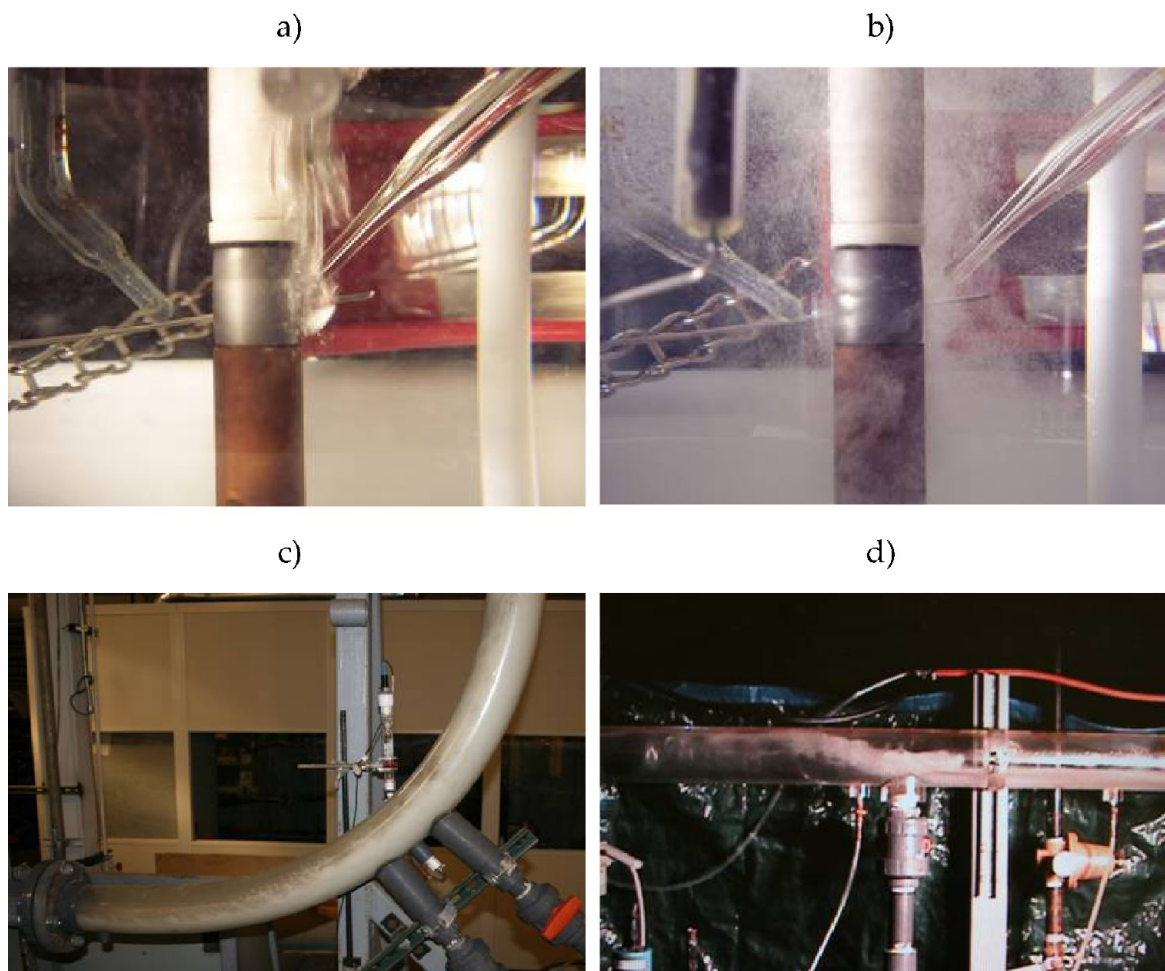


Figure 17. Examples of multiphase flow situations created to investigate the effect of wall shear stress on corrosion inhibitor performance: (a) water–gas impinging jet onto a rotating cylinder, (b) water–vapor impinging jet onto a rotating cylinder, (c) gas–water flow in an uphill pipe bend, (d) gas–water standing slug flow.

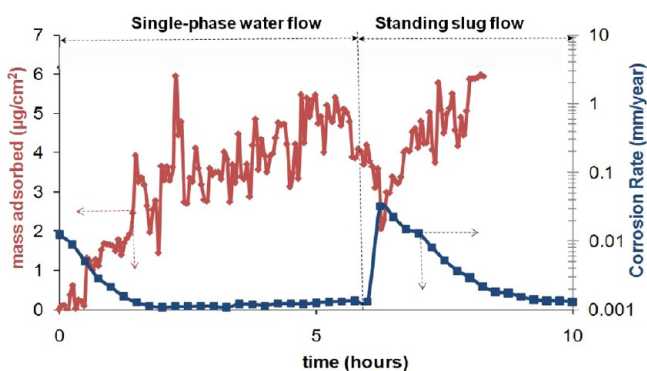


Figure 18. Measurements of adsorbed mass of a corrosion inhibitor using a quartz crystal microbalance and simultaneous measurements of the corrosion rate, for the case when pipe flow is changed from single-phase water flow to a standing-slug flow (see Figure 17d).

m/s. Actually, the opposite was found: mechanical erosion of the underlying steel was retarded by the presence of an inhibitor film, most likely by some sort of “micro-cushioning effect”.

In general, when inhibitor performance was found to be compromised permanently, factors other than mechanical forces were the cause, for example, inhibitor depletion because of foam formation in slug flow (see Figure 17c) or because of

adsorption onto sand particles, inhibitor degradation at high temperatures, etc.

Other Effects. Somewhat counterintuitively, there seems to be more problems with CO_2 corrosion of mild steel pipelines when the flow rate is low rather than high. For example, in wet gas pipelines, water and gas can stratify, leading to corrosion problems at the top of the pipe because of water condensation. In oil-carrying lines, even very small amounts of water may drop out to the bottom of the line, causing unexpected corrosion. Another example is the problem of settling of solids at low flow rates that leads to the so-called underdeposit attack. These are briefly described below. A more in-depth analysis exceeds the scope of this paper.

Effect of Water Condensation. TLC occurs in wet gas transportation and only in a stratified flow regime because of the condensation of water containing dissolved corrosive gases in the upper sections of the pipe. Condensation happens when the environment outside the pipeline is cooler than the saturated vapor flowing inside the pipe. The dissolution of corrosive gases, such as CO_2 , as well as condensation of acidic vapors, such as organic acids, lead to very aggressive conditions in the water droplets attached to the metal surface. The injection of chemical inhibitors, which is a standard method to combat corrosion issues in the settled water at the bottom of

the line, is not effective because inhibitors cannot reach the top of the line easily.

Effect of Water Wetting. In oil-carrying lines, there is usually some small amount of water. The two liquids, oil and water, can flow stratified or mixed. Low velocities lead to stratification of water and oil, with continuous water wetting of the pipe bottom, resulting in corrosion. If the amount of water is relatively small (<10%), a fast moving oil phase can entrain the water, which may lead to intermittent oil/water wetting or continuous oil wetting of the pipe walls. In the former case, the corrosion rate is much reduced, while in the latter case, there is no corrosion. Various crude oils have widely varying capacities to entrain water. Typically, it takes much higher flow rates for light oils to entrain water ($v > 1.5$ m/s) because of their lower density and viscosity. Some heavier oil are able to do the same at velocities as low as 0.5 m/s. However, chemical properties of crude oils, particularly the content of surface-active substances, are even more important for wetting behavior than their physical properties.

Immiscible fluids with high interfacial tension do not disperse as easily as fluids with low interfacial tension. Chemicals, such as inhibitors and emulsifiers, as well as polar compounds naturally occurring in the crude oil can gather at the oil–water interface and lower the interfacial tension. Naturally occurring compounds found in crude oil that have been found to have significant effects are those containing oxygen, sulfur, and nitrogen in their molecular structure. Furthermore, both asphaltenes and waxes have shown some positive inhibitive effects on corrosion.

Effect of Solids. The solids found in gas and oil pipelines are typically comprised of silica sand, clay, corrosion product, such as iron oxides or iron sulfides, mineral scales, such as calcium carbonate, precipitated waxes and asphaltenes, and inhibitor residuals. At low flow rates, these solids settle at the bottom of the pipe and can lead to so-called underdeposit corrosion. The steel under the deposits is harder to protect with conventional corrosion inhibitors, while in some cases, galvanic cells or even bacterial attack can aggravate the problem.

Erosion–corrosion occurs at very high flow velocities when the entrained solids cause erosion of protective layers and can even lead to damage of the underlying steel. However, the relatively low flow rates and the lack of flow disturbances in pipelines rarely give rise to erosion–corrosion problems.

CONCLUSION

Multiphase flow affects CO₂ corrosion of mild steel pipelines in a number of ways, with some of the most common effects being related to

(1) mass transfer, when an increased rate of turbulent mass transfer of corrosive species from the bulk solution leads to an acceleration of the corrosion rate and when an increased mass-transfer rate of the corrosion product away from the steel surface makes it harder to form protective ferrous carbonate layers;

(2) mechanical interactions, when the high wall shear stress allegedly removes the protective surface layers, such as iron carbonate or inhibitor films, and leads to localized attack; however, it was found using macroscopic as well as atomic-scale measurements (AFM) that, under typical pipeline conditions, the protective surface layers cannot be removed by mechanical forces alone;

(3) condensation in wet gas pipelines, which leads to a selective attack at the TLC, which is very difficult to inhibit;

(4) water settling in oil-carrying lines, when at low velocities water wetting can lead to serious corrosion problems even at very low water cuts; and

(5) sand production, which (a) at high velocities leads to erosion–corrosion and (b) at low velocities leads to sand settling and underdeposit corrosion.

AUTHOR INFORMATION

Corresponding Author

*E-mail: nestic@ohio.edu.

Notes

The authors declare no competing financial interest.

ACKNOWLEDGMENTS

The author is indebted to many individuals who contributed one way or another to the work reported above. The long list includes fellow scientist and researchers, corrosion engineers from the industry, as well as graduate students at the Institute for Corrosion and Multiphase Technology, Ohio University. Many are already listed in the list of references. In addition, special thanks go to Yao Xiong, Bruce Brown, Yang Yang, Jiabin Han, David Young, Azmi Mohammed Nor, and Christian Canto, all from Ohio University, Bernardo Molinas from Venezia Technologie, Valery Sheverev from Lenterra, Morten C. Langsholt and Knud Lunde from IFE, and Dominic Paisley from BP. Also, the author's gratitude goes to the many companies who have been supporting research efforts in CO₂ corrosion for a sustained period of time by providing continued guidance and funding to the Institute for Corrosion and Multiphase Technology, Ohio University. They are Baker Hughes, BG Group, BP, Champion Technologies, Chevron, Clariant, CNPC, ConocoPhillips, Encana, ENI, ExxonMobil, MI Swaco, Nalco, Occidental Oil and Gas, PDVSA, Petrobras, Petronas, PTT, Saudi Aramco, Shell, Tekioku Oil, Tenaris, Total, and Wood Group.

REFERENCES

- (1) Bonis, M. R.; Crolet, J. L. *Basics of the Prediction of the Risks of CO₂ Corrosion in Oil and Gas Wells*; NACE International: Houston, TX, 1989; Corrosion/89, Paper 466.
- (2) Nestic, S. Carbon dioxide corrosion of mild steel. In *Uhlig's Corrosion Handbook*, 3rd ed.; Winston Revie, R., Ed.; Wiley: New York, 2011; pp 229–247.
- (3) Nestic, S.; Sun, W. Corrosion in acid gas solutions. In *Shreir's Corrosion*, 4th ed.; Richardson, T. J. A., Cottis, B. R. A., Lindsay, R., Lyon, S., Scantlebury, D. J. D., Stott, H., Graham, M., Eds.; Elsevier: Amsterdam, The Netherlands, 2010; Vol. 2, pp 1270–1299.
- (4) Palmer, D. A.; van Eldik, R. *Chem. Rev.* **1983**, *83*, 651.
- (5) Drazic, D. M. Iron and its electrochemistry in an active state. *Aspects of Electrochemistry*; Plenum Press: New York, 1989; Vol. 19, p 79.
- (6) Lorenz, W.; Heusler, K. Anodic dissolution of iron group metals. In *Corrosion Mechanisms*; Mansfeld, F., Ed.; Marcel Dekker: New York, 1987.
- (7) Nešić, S.; Thevenot, N.; Crolet, J. L. *Electrochemical Properties of Iron Dissolution in CO₂ Solutions—Basics Revisited*; NACE International: Houston, TX, 1996; Corrosion/96, Paper 3.
- (8) Delahay, P. *J. Am. Chem. Soc.* **1952**, *74*, 3497.
- (9) de Waard, C.; Milliams, D. E. *Corrosion* **1975**, *31*, 131.
- (10) Gray, L. G. S.; Anderson, B. G.; Danysh, M. J.; Tremaine, P. G. *Mechanism of Carbon Steel Corrosion in Brines Containing Dissolved Carbon Dioxide at pH 4*; NACE International: Houston, TX, 1989; Corrosion/89, Paper 464.
- (11) Eriksrud, E.; Søntvedt, T. Effect of flow on CO₂ corrosion rates in real and synthetic formation waters. In *Advances in CO₂ Corrosion*;

Hausler, R. H., Goddard, H. P., Eds.; NACE International: Houston, TX, 1984; Vol. 1, p 20.

(12) Schmitt, G.; Rothman, B. *Werkst. Korros.* **1977**, *28*, 816.

(13) Gray, L. G. S.; Anderson, B. G.; Danysh, M. J.; Tremaine, P. R. *Effect of pH and Temperature on the Mechanism of Carbon Steel Corrosion by Aqueous Carbon Dioxide*; NACE International: Houston, TX, 1990; Corrosion/90, Paper 40.

(14) Nešić, S.; Postlethwaite, J.; Olsen, S. An electrochemical model for prediction of the corrosion of mild steel in aqueous CO₂ solutions. *Corrosion* **1996**, *52*, 280.

(15) Nešić, S.; Pots, B. F. M.; Postlethwaite, J.; Thevenot, N. Superposition of diffusion and chemical reaction limiting currents—Application to CO₂ corrosion. *J. Corros. Sci. Eng.* **1995**, *1*, No. 3, http://www.cp.umist.ac.uk/JCSE/Vol1/PAPER3/V1_p3int.htm.

(16) Sun, W.; Nešić, S. Kinetics of corrosion layer formation, part 1. Iron carbonate layers in carbon dioxide corrosion. *Corrosion* **2008**, *64*, 334.

(17) Sun, W.; Nešić, S.; Woollam, R. C. The effect of temperature and ionic strength on iron carbonate (FeCO₃) solubility limit. *Corros. Sci.* **2009**, *51*, 1273.

(18) Nešić, S.; Solvi, G. T.; Enerhaug, J. *Corrosion* **1995**, *51*, 773.

(19) Schmitt, G. A.; Mueller, M.; Papenfuss, M.; Strobel-Effertz, E. *Understanding Localized CO₂ Corrosion of Carbon Steel from Physical Properties of Iron Carbonate Scales*; NACE International: Houston, TX, 1999; Corrosion/99, Paper 38.

(20) Gulbrandsen, E.; Nesic, S.; Stangeland, A.; Burchardt, T. *Effect of Precorrosion on the Performance of Inhibitors for CO₂ Corrosion of Carbon Steel*; NACE International: Houston, TX, 1998; Corrosion/98, Paper 13.